INTERNATIONAL JOURNAL FOR NUMERICAL METHODS IN FLUIDS, VOL. 19, 415–437 (1994)

STABILITY OF A NUMERICAL ALGORITHM FOR GAS BUBBLE MODELLING

M. R. BARKHUDAROV* AND S. B. CHIN†

* *Department of Engineering Materials, † Department of Mechanical and Process Engineering, The University of Sheffield, Mappin Street, Sheffield, S1 4DU, U.K.*

SUMMARY

A free-surface-tracking algorithm based on the SOLA-VOF method is analysed for numerical stability when modelling gas bubble evolution in a fluid. It is shown that an instability can arise from the fact that the bubble pressure varies with its volume. A time step stability criterion is introduced which is a function of the natural oscillation period but does not depend on the mesh size. This dependence suggests that the instability is likely to arise in the case of a general motion of a bubble, especially if break-up occurs. The effect is shown using linear Fourier analysis of the discretized equation for radial bubble oscillation and demonstrated numerically using a CFD code FLOW-3D. One- and three-dimensional situations are considered: a bubble in a fluid bounded by two concentric surfaces and a bubble floating in a fluid chamber with and without gravity. In cases where no analytical solution is available, a numerical method for the stability time step limit calculation is suggested based on finding the natural oscillation frequency.

The nature of the instability suggests that it can be a feature of any numerical algorithm which models transient fluid flow with a free surface.

KEY WORDS Bubbles Free surface Finite volume Numerical stability

1. INTRODUCTION

There have been many studies, both experimental and theoretical, devoted to the behaviour of gas bubbles in liquids. Walters and Davidson provided detailed experimental descriptions of large cylindrical[1] and spherical[2] bubbles floating in liquid chambers. Vokurka[3] gave a comprehensive review of the experimental work and methods for its evaluation and suggested a classification of freely oscillating bubbles in terms of oscillation amplitudes.

The theoretical work has mainly been confined to studying steady flows or flows with small perturbations.[4,5] Recently Yang *et al.*[6] made an extensive study of non-linear effects of oscillations of a large spherical bubble submerged in a uniform axisymmetrical flow. They showed that the radial ('breathing') wave mode interacts with the shape deformation modes to create resonances. The shape deformation oscillations occur either owing to the mean flow or owing to a pressure pulse in a quiescent fluid; in both cases a non-uniform pressure distribution on the bubble surface is generated.

The relatively recent developments in the numerical techniques and computer hardware have enabled the simulation of bubble motion in a general case. An important part of a numerical simulation is the tracking of the free surface and defining boundary conditions on it. In the absence of gas–fluid mass exchange the boundary conditions are

$$\partial S/\partial t + \mathbf{u}\cdot\nabla S = 0, \qquad p_b + \sigma\zeta = p_s - 2\mu\partial u_n/\partial n, \tag{1}$$

CCC 0271–2091/94/170415–23

Received July 1993
Revised January 1994

where S is a free surface element, p_b and p_s are the bubble and fluid pressures at the surface respectively, σ is the surface tension coefficient, ζ is the local surface curvature and u_n is the fluid velocity projection on the surface normal $\mathbf{n}$.

Ryskin and Leal[7,8] employed a boundary-fitting technique in which the free surface coincides with a grid line and applied the technique to steady state flows. The same method was applied by Kang and Leal[9] for transient axisymmetric and biaxial straining flows for a range of Reynolds and Weber numbers.

Another approach to free surface problems is to model the motion of both fluid and gas by introducing a density discontinuity at the free surface.[10] In this case the equations of motion are solved over the entire gas–fluid domain. Special care has to be taken in preserving the sharpness of the discontinuity front, e.g. by using a higher-order discretization scheme. However, for large differences in liquid and gas densities ($\rho_L/\rho_G \approx 1000$) and large Reynolds numbers the motion of the gas inside the bubble becomes unimportant and the pressure distribution in it can be assumed uniform.

Bugg and Rowe[11] used the SOLA-VOF method to model the evolution of large cylindrical and spherical bubbles ascending in a liquid chamber. Their results showed good agreement with experimental data. The SOLA-VOF method[12] evolved from the marker-and-cell (MAC) technique[13] and uses the fraction-of-fluid function F to describe the free surface location and motion. It is now widely used for various applications involving transient free boundaries.

The present work is concerned with the radial or 'breathing' wave mode of a bubble submerged in an ideal, incompressible fluid in one and three dimensions. The equations of motion of the fluid in these cases can be reduced to a single equation describing linear waves. It is shown that a numerical method of solving this equation is only conditionally stable if the free surface boundary condition is approximated explicitly. The maximum time step is a function of only the wave period. In an implicit method the position of the free surface is coupled with the fluid pressure and velocity. Although this makes the calculation unconditionally stable, it introduces a numerical diffusion which varies with the time step.

The theoretical analysis is supported by simulations using a general-purpose CFD package FLOW-3D.* The main feature of the code is its ability to simulate multiple free surfaces in three dimensions using an algorithm based on the SOLA-VOF method. It is employed here to investigate the stability properties of the method in the case when the bubble pressure varies according to $pV^\gamma = \text{const}$.

2. ANALYSIS

2.1. Basic equation

Consider the radial motion of an isolated symmetrical gas bubble of radius $R(t)$ in an incompressible fluid bounded by a concentric spherical free surface of radius $r_0 > R(t)$, where the pressure is constant and equal to p_0 as shown in Figure 1.

We will restrict the analysis here to the case of large Reynolds numbers,

$$N_{Re} = 2RU\rho/\mu \gg 1,$$

where ρ is the fluid density, U is the fluid characteristic velocity and μ is the fluid viscosity coefficient. In other words, the influence of the fluid viscosity will be neglected compared with

* Property of Flow Science Inc., Los Alamos, NM.

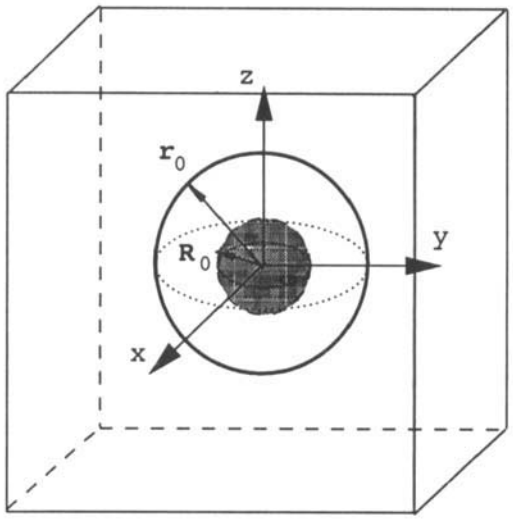

Figure 1. Spherical bubble of radius R_0 (shaded region) and concentric fluid region of radius r_0 used to describe one-dimensional radial wave mode

that of the surface tension and inertia. Physically this corresponds to large bubbles floating in a low-viscosity liquid.[14]

Conditions (1) at the bubble surface can now be written as

$$u(R) = \mathrm{d}R/\mathrm{d}t = \dot{R}, \tag{2}$$

$$p(R) = p_b - 2\sigma/R, \tag{3}$$

where p_b is the gas pressure inside the bubble.

For simplicity the radius r_0 will be considered large enough to neglect surface tension at the outer free surface, so that

$$p(r_0) = p_0. \tag{4}$$

To derive the equation for $R(t)$, a fluid control volume is introduced at time t with boundaries at $r_1 = R(t)$ and $r_2 = r_0$. The kinetic energy conservation principle for an incompressible fluid applied to this control volume, with boundary conditions (2)–(4), yields the following equation for R.[15]

$$\frac{\mathrm{d}}{\mathrm{d}t}\left[\dot{R}^2\left(R^3 - \frac{R^4}{r_0}\right)\right] = R^2\dot{R}\,\frac{2}{\rho}\left(p_b - \frac{2\sigma}{R} - p_0\right). \tag{5}$$

For an ideal gas the bubble pressure p_b varies with its volume V as

$$p_b/p_{b_0} = (V_0/V)^\gamma = (R_0/R)^{3\gamma}, \tag{6}$$

where the parameter γ varies between unity for an isothermal gas and the ratio C_p/C_v of the gas specific heats for an adiabatic process (e.g. $C_p/C_v = 1{\cdot}4$ for air). To simplify the analysis, we will assume that p_{b_0} and V_0 are the equilibrium bubble pressure and volume respectively, i.e.

$$p_{b_0} - 2\sigma/R = p_0,$$

and consider motions of the bubble which are small deviations from equilibrium:

$$x(t) = [R(t) - R_0]/R_0 \ll 1.$$

Then, omitting all terms of order higher than one and rearranging, we obtain the linearized form of equation (5) as

$$\ddot{x} + a^2 x = 0, \tag{7}$$

where

$$a^2 = (3\gamma p_{b_0} - 2\sigma/R_0)/R_0^3\rho(1/R_0 - 1/r_0). \tag{8}$$

Similar derivations for one-dimensional cylindrical and planar geometries also yield equation (7). For the cylindrical case

$$a^2 = (2\gamma p_{b_0} - \sigma/R_0)/R_0^2\rho \ln (r_0/R_0). \tag{9}$$

and for the planar motion

$$a^2 = \gamma p_{b_0}/R_0\rho(r_0 - R_0). \tag{10}$$

The main difference between these cases is the dependence of a^2 on the fluid dimensions and on the bubble radius. Also, an oscillating solution for infinite fluid thickness ($r_0 \to \infty$) only exists in the spherical case:

$$a_\infty^2 = (3\gamma p_{b_0} - 2\sigma/R_0)/R_0^2\rho. \tag{11}$$

Equation (7) describes linear natural oscillations with period

$$\mathscr{T} = 2\pi/a. \tag{12}$$

2.2. Numerical analysis

We will apply a numerical method to solve equation (7). If the time axis is divided into equal increments of size Δt starting at $t = 0$, then, applying first-order backward differencing, at time $t = (k + 1)\Delta t$ we have

$$(x^{k+1} - 2x^k + x^{k-1})/\Delta t^2 + a^2 x^l = 0. \tag{13}$$

Here $x^k = x(k\Delta t)$. If $l = k$, then the position of the free surface, hence the bubble pressure, is included in the calculation explicitly; if $l = k + 1$, then the calculation becomes implicit. Fourier analysis, in which the solution of equation (13) is sought in the form

$$x^k = e^{\lambda k \Delta t},$$

where λ is a complex number and

$$\text{Real}(\lambda) \leqslant 0$$

is required for numerical stability, shows that the explicit method is stable if

$$\Delta t \leqslant \Delta t_{max} = 2/a = \mathscr{T}/\pi, \tag{14}$$

while the implicit method is unconditionally stable. Unlike most of the other stability criteria, the left-hand side of equation (14) does not depend on the grid size but is a function of the natural oscillation period $\mathcal{T}$.

Numerical diffusion is absent in the explicit method for stable time step sizes, i.e.

$$\text{Real}(\lambda) = 0,$$

while the implicit method algorithm does introduce numerical diffusion because

$$\text{Real}(\lambda) = -(1/2\Delta t)\ln(1 + \Delta t^2 a^2) < 0, \tag{15}$$

with a maximum diffusion at $\Delta t \approx 1{\cdot}98/a$.

Equations (8)–(10) for a^2 can be rewritten in the form

$$a^2 = c_0[N\gamma p_{b_0} - (N-1)\sigma/R_0]/V_0 m, \tag{16}$$

where for the spherical geometry

$$N = 3, \qquad c_0 = 4\pi/3, \qquad m = \rho(1/R_0 - 1/r_0),$$

for the cylindrical geometry

$$N = 2, \qquad c_0 = \pi, \qquad m = \rho \ln(r_0/R_0),$$

for the planar geometry

$$N = 1, \qquad c_0 = 1, \qquad m = \rho(R_0 - r_0)$$

and V_0 is the bubble volume. The parameter m may be used as a measure of the fluid inertia.

Now it is clear how different characteristics influence the numerical stability criterion given by equation (14). For example, a smaller bubble volume or fluid density will decrease the maximum time step size. The same is true for a larger bubble 'stiffness' γp_{b_0}.[16]

The main influence of the bubble geometry is shown by the expression for m. In general, the maximum time step size may be increased by increasing the volume of fluid around the bubble (e.g. by increasing r_0). There is no upper limit for Δt_{max} for the cylindrical and planar geometries as $r_0 \to \infty$. However, this is not the case for the spherical geometry. Equation (11) shows that the dependence of a on r_0 decreases rapidly as r_0 grows and eventually vanishes when $r_0 \to \infty$, so that even for an infinite volume of fluid there is a finite stability limit. This means that spherical bubbles are perhaps the most difficult to model numerically using the explicit method.

3. NUMERICAL SOLUTION METHOD

For the numerical simulation the discretized partial differential equations of motion for the fluid are solved. For an ideal incompressible fluid the equations are

$$\partial \mathbf{u}/\partial t + (\mathbf{u}\cdot\nabla)\mathbf{u} = -(1/\rho)\nabla p, \tag{17}$$

$$\nabla\cdot\mathbf{u} = 0. \tag{18}$$

To determine the position of the free surface, the following equation is solved for the fluid fraction function:

$$\partial F/\partial t + (\mathbf{u}\cdot\nabla)F = 0. \tag{19}$$

A finite volume first-order upwind differencing scheme is employed to solve equations (17)–(19) in three dimensions using a non-uniform mesh of rectangular cells. Owing to the

incompressibility of the fluid, the pressure has to be approximated implicitly at each time step to avoid numerical instability. The resulting linear algebraic equations for pressure and velocity are solved iteratively using the successive overrelaxation (SOR) method.[17] A detailed description of the numerical algorithm can be found elsewhere.[11,12] Here we will briefly outline the main steps. At each time step the following steps are performed.

1. New, first-guess velocities are calculated from the momentum equations using old pressures.
2. Since in general these velocities will not satisfy the continuity equation (18), an adjustment is made to the pressure in full cells only. This adjustment introduces a correction to the cell velocity so that the continuity equation is satisfied exactly.
3. Step 2 carried out in a cell will upset the mass balance in its neighbours and the procedure has to be repeated until the divergence of the velocity in all cells is smaller than a predefined parameter ϵ.
4. Equation (19) is solved for F by a donor–acceptor advection method using the new velocities.

In the cells which contain a free surface the interface is approximated by a flat surface parallel to the nearest co-ordinate plane. In the original SOLA-VOF method the pressure in the surface cells was obtained by linear interpolation between the free surface and the neighbouring full cell. In the present work the surface cell pressure is estimated by assuming a hydrostatic pressure distribution between the free surface and the cell centre. The pressure gradient in the cell is defined by the body forces normal to the surface, such as gravity and inertia. The advantage of this method in the elimination of possible instabilities arising either from the interpolation procedure or in a situation when the same full cell is used to define pressures in two or more surface cells. The latter is especially likely to happen in three-dimensional problems.

Waves on the free surface can also lead to a numerical instability associated with the propagation of these waves. If a body force f_b is applied to the fluid in a direction normal to the free surface, there may be surface waves with speeds of order $\sqrt{(hf_b)}$, where h is the depth of fluid or the wavelength. In the simulation the cell size in the direction normal to the free surface is used for h in each surface cell. The numerical stability condition requires that surface waves should not propagate more than one cell in one time step. For example, if z is the normal direction to the surface and f_{b_z} is the normal body force, then

$$\Delta t < \min_{i,j}(\Delta x_i, \Delta y_j)/\sqrt{(f_{b_z}\Delta z_k)}. \tag{20}$$

Note that the right-hand side of (20) is mesh-dependent.

At each time step the free surface is not adjusted during the iteration procedure, its position being fixed at the previous time step. This effectively means that the free surface boundary condition is included explicitly.

Analytical results of Section 2.2, where an equation for one control volume encompassing the whole fluid region was analysed, can be applied to the present numerical method even though it uses a number of smaller control volumes. This is because the same conservation laws and boundary conditions are used in both approaches.

In fact, any CFD code which can describe the 'breathing' wave mode should have the bubble instability problem as an intrinsic feature of the numerical method, unless the fluid free surface is included in the calculation implicitly.

Although there is a fixed upper limit for the time step in the cases considered in Section 2, it is difficult to find this limit in the case of general bubble motion with non-symmetrical deformations and break-up. For this reason an implicit method was developed to model bubbles.

The implicit algorithm estimates the position of the free surface at each iteration by applying the latest velocities to the free surface cells to obtain the approximate position of the free surface. Then the bubble volume and pressure are estimated and the free surface boundary condition is updated for the next iteration. This method is fast since it calculates only surface cell movement and does not solve the equation for the fluid fraction function F in the whole domain during iteration.

This development solves the instability problem in many practical cases, though it is recognized that it does not eliminate it completely. The flow can still become unstable if the bubble is too 'stiff', i.e. small volume variations (e.g. around 1%, which is within the resolution error) cause bubble pressure changes out of limits of the physical problem. In this case truncation errors in approximating the bubble surface can produce such an effect. If the volume of such a bubble changes little during the whole simulation, then it could be treated as an incompressible fluid using an appropriate numerical algorithm, e.g. a two-fluid flow algorithm.

4. NUMERICAL RESULTS

In this section simulations of cylindrical bubble oscillations are presented. The choice of the geometry is only dictated by the ease of the calculation and postprocessing in a cylindrical co-ordinate system.

The following input parameters are used as the basic set of values:

$$R_0 = 5 \text{ cm}, \qquad r_0 = 10 \text{ cm}, \tag{21}$$

$$p_0 = 1{\cdot}0 \times 10^6 \text{ dyn cm}^{-2}, \qquad p_{b_0} = 1{\cdot}01 \times 10^6 \text{ dyn cm}^{-2}, \tag{22}$$

$$\gamma = 1{\cdot}4, \qquad \rho = 4 \text{ kg cm}^{-3}, \qquad \sigma = 300{\cdot}0 \text{ dyn cm}^{-1}. \tag{23}$$

The difference between the bubble and ambient pressures, $\Delta p = 0{\cdot}01 \times 10^6$ dyn cm^{-2}, at the beginning of the calculation serves as the initiator of the fluid motion. Since Δp constitutes only 1% of p_0, the movement is expected to consist of small displacements of the fluid from its equilibrium, governed by equation (7).

Using equations (9), (12) and (14), we have

$$a = 201 \text{ s}^{-1}, \qquad \Delta t_{\max} = 0{\cdot}01 \text{ s}, \qquad \mathscr{T} = 0{\cdot}0313 \text{ s}.$$

The convergence criterion $\epsilon = 1{\cdot}0 \times 10^{-6}$ s^{-1} was used to ensure both sufficient speed and accuracy of the simulation. The bubble pressure and fluid mean kinetic energy are recorded at each time step as indicators of numerical stability.

4.1. Boundary condition accuracy

Cylindrical co-ordinates are introduced in such way that the free surfaces at $r = R_0$ and $r = r_0$ are aligned with mesh iso-surfaces $r = \text{const}$. The computational domain includes a sector of the bubble and fluid, as shown in Figure 2, with $0 \leqslant r \leqslant 15$ cm.

First a number of calculations using the explicit algorithm (all calculations below are explicit unless stated otherwise) were performed for a uniform mesh with the cell number in the r-direction, N, varying between 4 and 30 ($N < 4$ does not give enough resolution to describe the oscillations) and $\alpha = \Delta t/\Delta_{\max} = 0{\cdot}1$ to test the sensitivity of the result to N. The bubble pressure oscillations for $N = 5$ are shown in Figure 3. As expected, the wave amplitude does not show any decay and is equal to the initial pressure difference Δp.

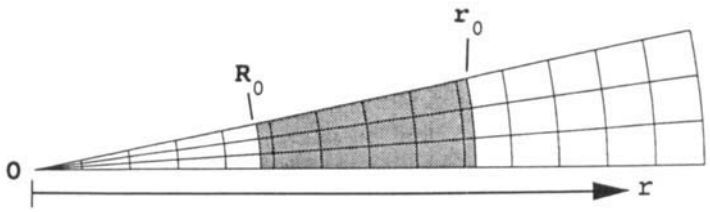

Figure 2. Section of cylindrical bubble of radius R_0 and mesh ($N = 14$) used for numerical simulations. 0 is the bubble centre and the shaded region highlights the fluid

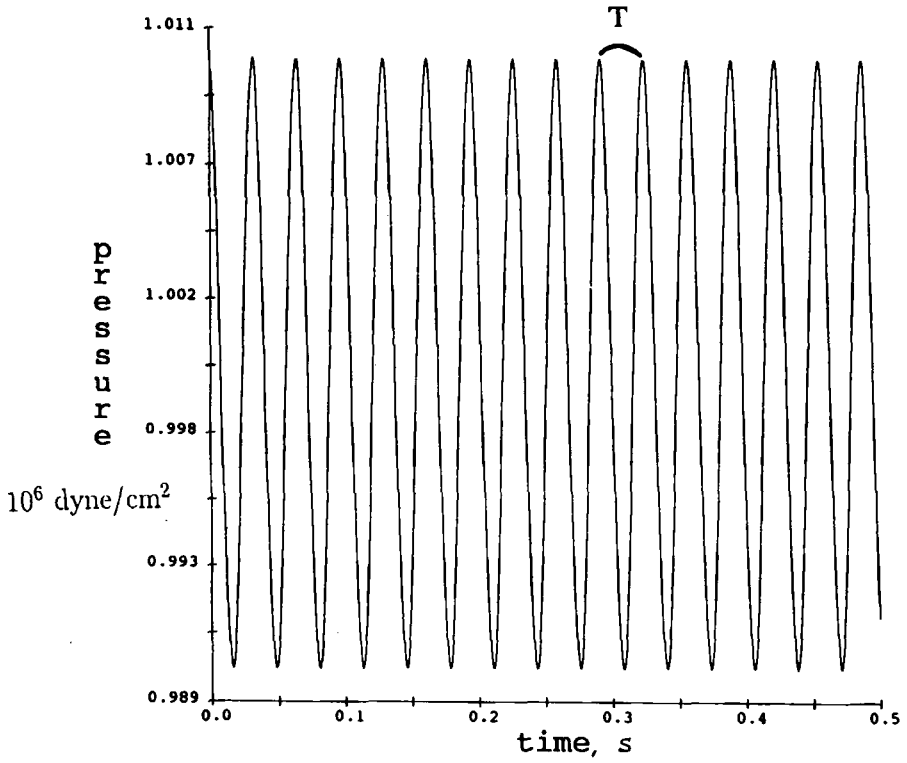

Figure 3. One-dimensional cylindrical bubble pressure oscillation with period $\mathcal{T}$ for $N = 5$ and $\Delta t = 0{\cdot}001$ s ($\alpha = 0{\cdot}1$). Explicit method

The amplitude does not depend on the mesh size, but the period $\mathcal{T}_N$ does vary with N. Figure 4 shows the relative error

$$\mathcal{T}_{\text{err}} = (\mathcal{T}_N - \mathcal{T}_{\text{analytical}})/\mathcal{T}_{\text{analytical}}$$

plotted against N. The error asymptotically converges to zero as N grows. For the minimum number of cells, $N = 4$, the error is within 15% of the analytical solution and for $N > 13$ it becomes less than 4%.

The mismatch occurs because, in the absence of a body force, the surface pressure is transferred

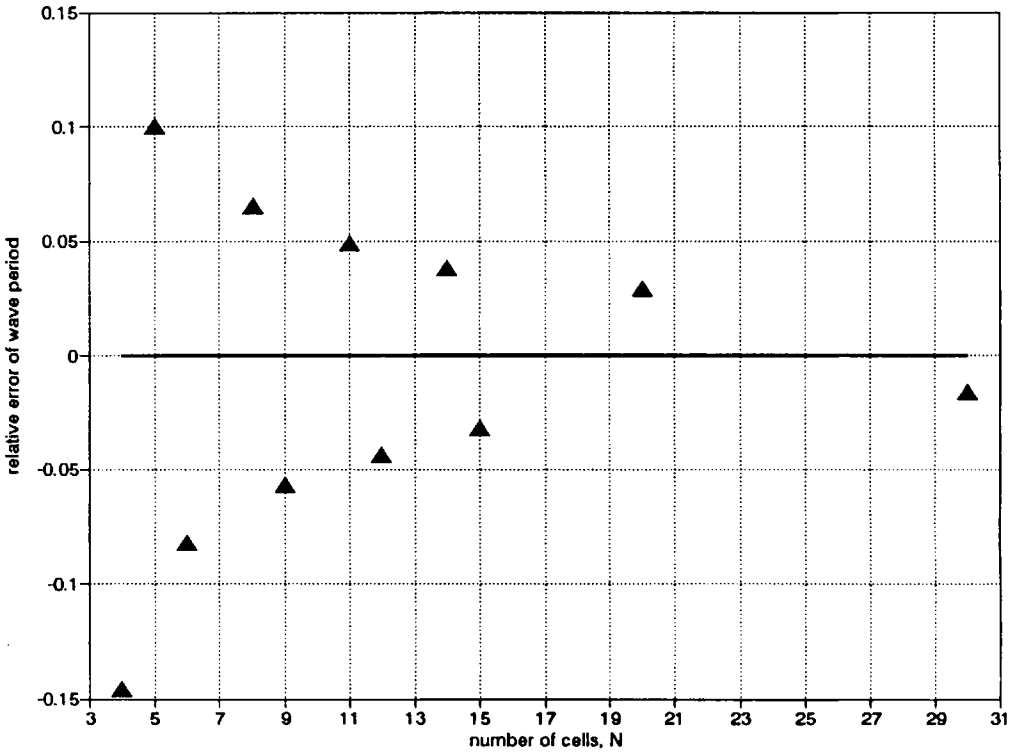

Figure 4. Relative error of computer simulations of wave period $\mathcal{T}_{err} = (\mathcal{T}_N - \mathcal{T})/\mathcal{T}$ as a function of cell number N in radial direction for one-dimensional cylindrical bubble. Explicit method, $\alpha = 0{\cdot}1$

unchanged from the free surface to the cell centre. This effectively distorts the pressure gradient between the inside and outside fluid boundaries. The sign of the error depends on whether a surface cell centre is covered with fluid or not, i.e. whether the pressure is shifted inwards (lower predicted periods) or outwards (higher predicted periods) of the fluid.

4.2. One-dimensional flow

The simulations of the one-dimensional flow employed the $N = 14$ mesh and the cells size $\Delta x = \frac{15}{14}$ cm is maintained throughout the rest of the paper.

The domain shown in Figure 2 is used to investigate the dependence of the stability of the calculation on the time step size. The total simulation time is 0·5 s. For $N = 14$ the calculated wave period is

$$\mathcal{T}_N = 0{\cdot}0324 \text{ s}, \tag{24}$$

which is 3·5% larger than the analytical value (for the reason given in Section 4.1). This means that the time step stability limit is also 3·5% larger and equal to $\Delta t_{\max_N} = 0{\cdot}01035$ s.

Figure 5 shows the fluid mean kinetic energy behaviour for the first 0·1 s for four values of α. The value $\alpha = 0{\cdot}1$ gives a non-decaying wave close to the analytical solution. The onset of instability is clearly seen when $\alpha = 1{\cdot}06$. However, the amplitude stabilizes after the rapid growth in the first 0·05 s, because the flow velocity becomes so high that the time step is reduced to

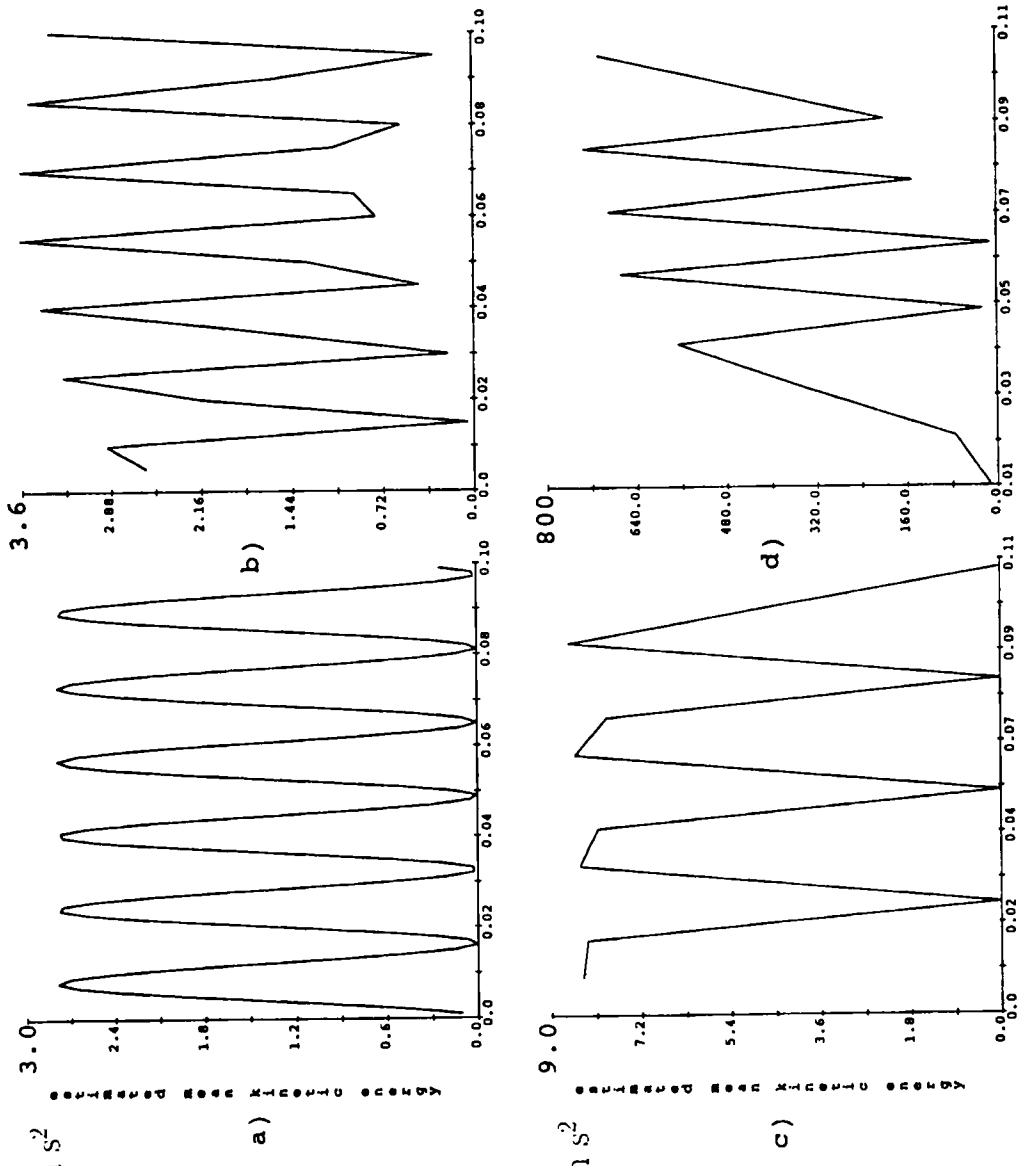

Figure 5. Mean fluid kinetic energy evolution with time for (a) $\alpha = 0{\cdot}1$, (b) $\alpha = 0{\cdot}5$, (c) $\alpha = 0{\cdot}9$ and (d) $\alpha = 1{\cdot}06$ using explicit method. When $\alpha > 1$, the calculation becomes unstable

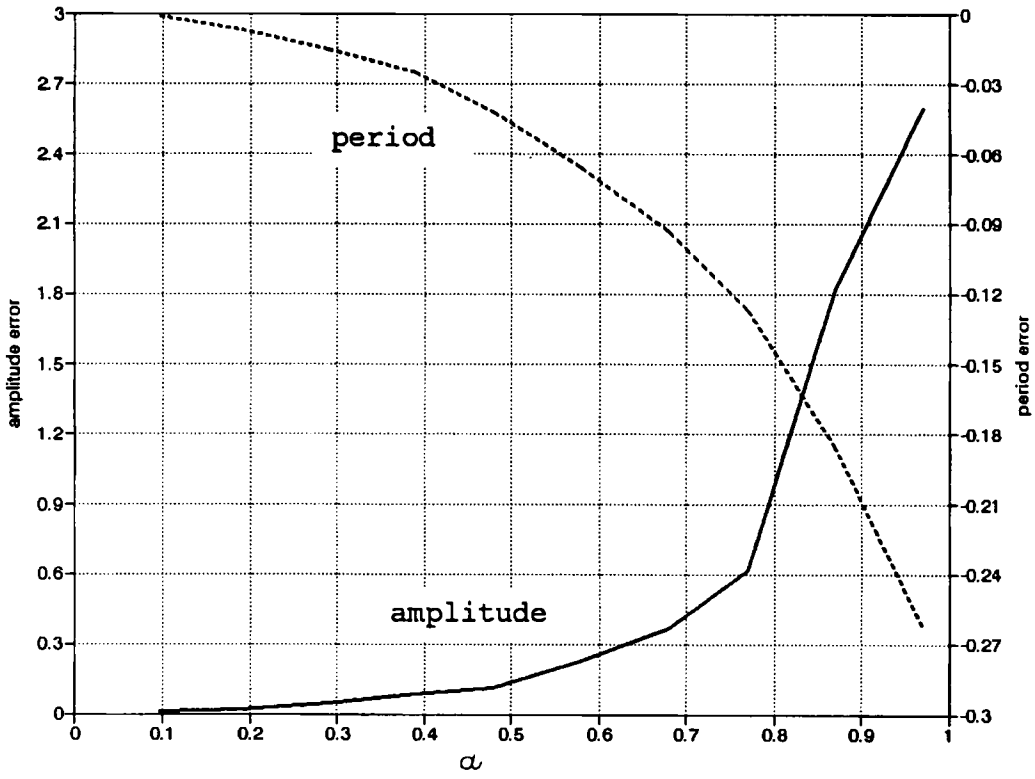

Figure 6. Relative numerical errors for wave amplitude $[A(\alpha) - A_0]/A_0$, and period, $[\mathscr{T}(\alpha) - \mathscr{T}_N]/\mathscr{T}_N$, as functions of α. A_0 is the exact analytical solution and $\mathscr{T}_N$ is the numerical solution for a small time step size with $\alpha = 0{\cdot}0001$. Explicit method, $N = 14$

satisfy the Courant stability criterion. The latter is triggered automatically during the calculation. The apparent variation in the amplitude with time for $\alpha = 0{\cdot}5$ and $0{\cdot}9$ is due to the postprocessing interpolation errors.

Figure 6 shows the dependence of the relative errors of the predicted wave amplitude, $(\mathscr{T} - \mathscr{T}_N)/\mathscr{T}_N$, and period, $(A - A_0)/A_0$, on α in the stable range. A_0 is the exact analytical solution for the amplitude, while the period $\mathscr{T}$ is normalized by $\mathscr{T}_N$ given by equation (24), because for a given mesh, as $\Delta t \to 0$, $\mathscr{T}$ converges to $\mathscr{T}_N$. Note that although the period varies with the time step size, the stability criterion is still defined by $\mathscr{T}_N$.

The instability can be avoided for a given time step by increasing Δt_{max}. This can be achieved, for example, by reducing both the ambient pressure p_0, and the bubble pressure p_{b_0}, by a factor of four. In this case, according to equations (9) and (14), for the given surface tension coefficient the maximum time step will approximately double and, for the same Δt, $\alpha = 0{\cdot}53$, thus ensuring stability. The result is shown in Figure 7 (compare with Figure 5(d)). Note that the wave period has also doubled.

Another way of avoiding the instability is to employ the implicit algorithm described in Section 3. Figure 8(a) shows the mean kinetic energy evolution for the input data given by equations (21)–(23) and $\alpha = 1{\cdot}06$. Initially the mean kinetic energy increases rather steeply but

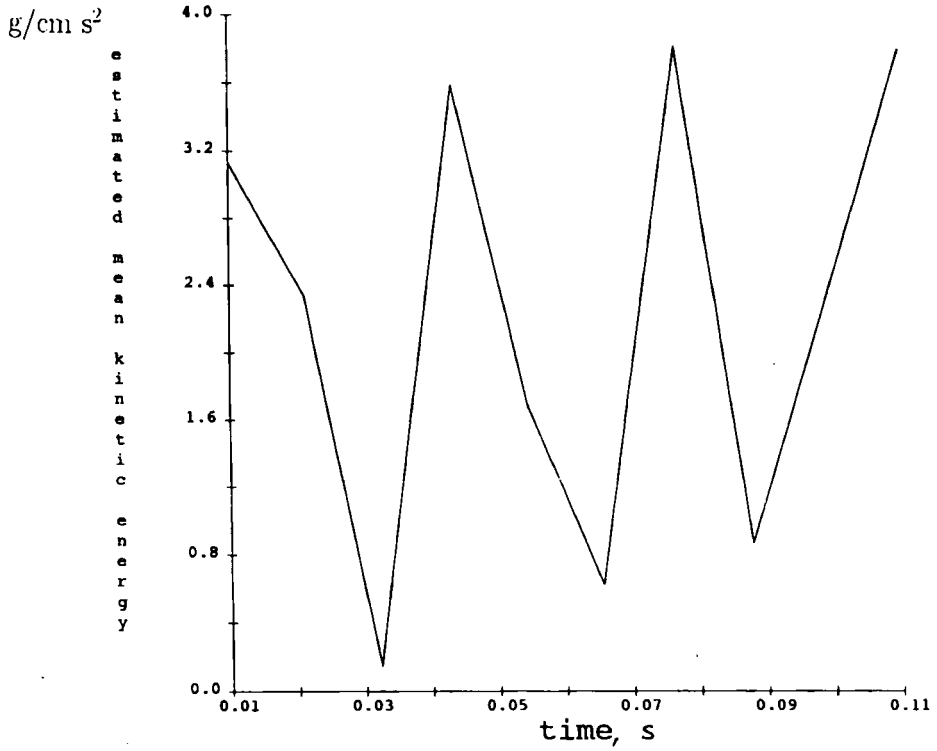

Figure 7. Same as Figure 5(d) but with bubble stiffness γp_{b_0} reduced by a factor of four so that $\alpha = 0{\cdot}53$

then the oscillations decay quickly to zero within a few time steps. The results show a dissipation of the fluid energy due to the numerical diffusion inherent in the implicit method. The wave decay grows as α increases from 0·01 to 0·5 in Figure 8, in agreement with the analytical results. It follows from equation (15) that the amplitude is halved every

$$I = 2\alpha \ln 2/\pi \ln (1 + 4\alpha^2)$$

wave periods. For example, for $I > 10$ it is necessary that $\alpha < 0{\cdot}011$.

4.3. Three-dimensional Flow

Bugg and Rowe[11] showed that the SOLA-VOF method can be successfully used to model the movement of gas bubbles floating towards the free surface in a fluid vessel. Bubble oscillations cannot be reduced only to the radial mode. Shape deformation modes will also be present. In a linear approximation these waves do not alter the bubble volume, so that fluctuations of the bubble pressure can be attributed to the 'breathing' mode only.

Consider an arbitrary bubble of volume V_0 submerged in a fluid chamber surrounded by solid walls at $x = x_1$, $x = x_2$, $y = y_1$, $y = y_2$ and $z = -z_0$ and by a horizontally free surface at $z = 0 > -z_0$ as shown in Figure 9, together with the mesh used in the simulations. As in the one-dimensional case in Section 2.1, the outer free surface is open to the atmosphere at a constant pressure p_0 and p_b is the bubble pressure.

Natural 'breathing' mode oscillations will be considered here in the absence of gravity. If the

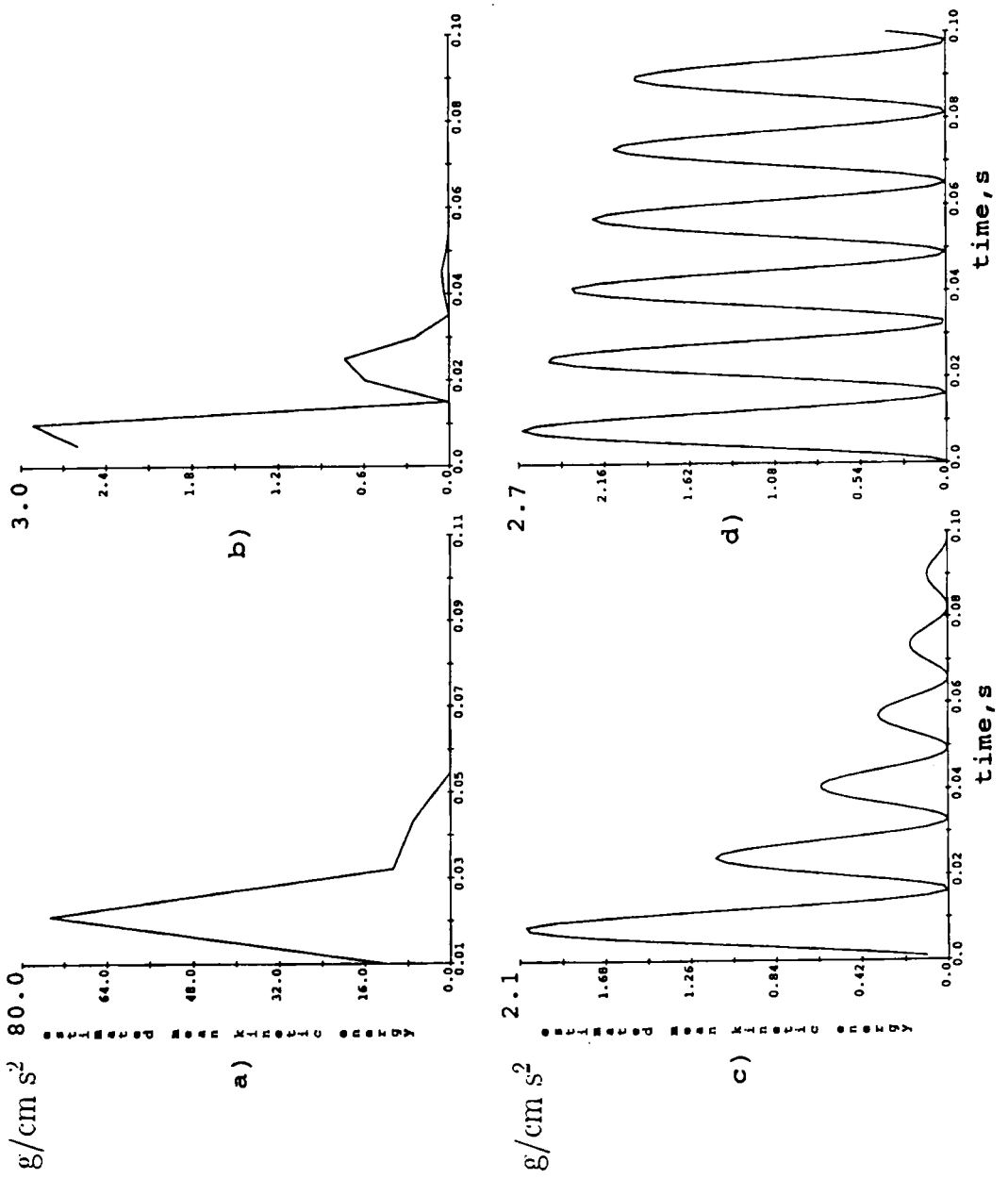

Figure 8. Mean fluid kinetic energy evolution with time for (a) $\alpha = 1{\cdot}06$, (b) $\alpha = 0{\cdot}5$, (c) $\alpha = 0{\cdot}1$ and (d) $\alpha = 0{\cdot}01$ using implicit method

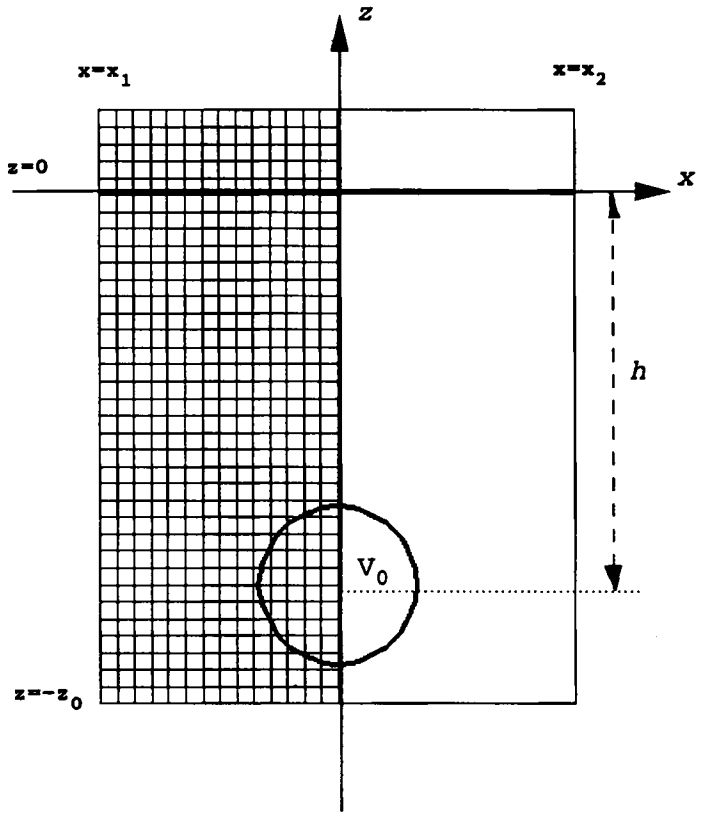

Figure 9. Geometrical set-up and mesh for two-dimensional problem of a bubble of initial volume V_0 in a fluid chamber. Only half of the whole domain was used for the numerical simulations owing to the symmetry

oscillation period is known, then the time step stability limit is defined by equation (14). There is no exact analytical solution available to describe the linear waves in this case, but an approximate expression could be obtained.

Let $z = -h$ denote the horizontal plane that passes through the geometrical centre of the bubble. The two simplifying assumptions that help us to derive an equation for the oscillations are as follows.

Assumption 1. The kinetic energy of the fluid lying below $z = -h$ is negligible compared with that of the fluid above the plane, so that only the motion of the latter will be considered.

Assumption 2. All the fluid in the region $z > -h$ moves at a uniform vertical velocity $w = \dot{z}$, so that the fluid/air interface stays flat and parallel to $z = 0$.

A deeply submerged bubble in a narrow vessel would correspond to these assumptions most closely.

The volume of fluid lying between $z = 0$ and the fluid/air interface is

$$V_{fl} = A_0 h - \tfrac{1}{2} V_0,$$

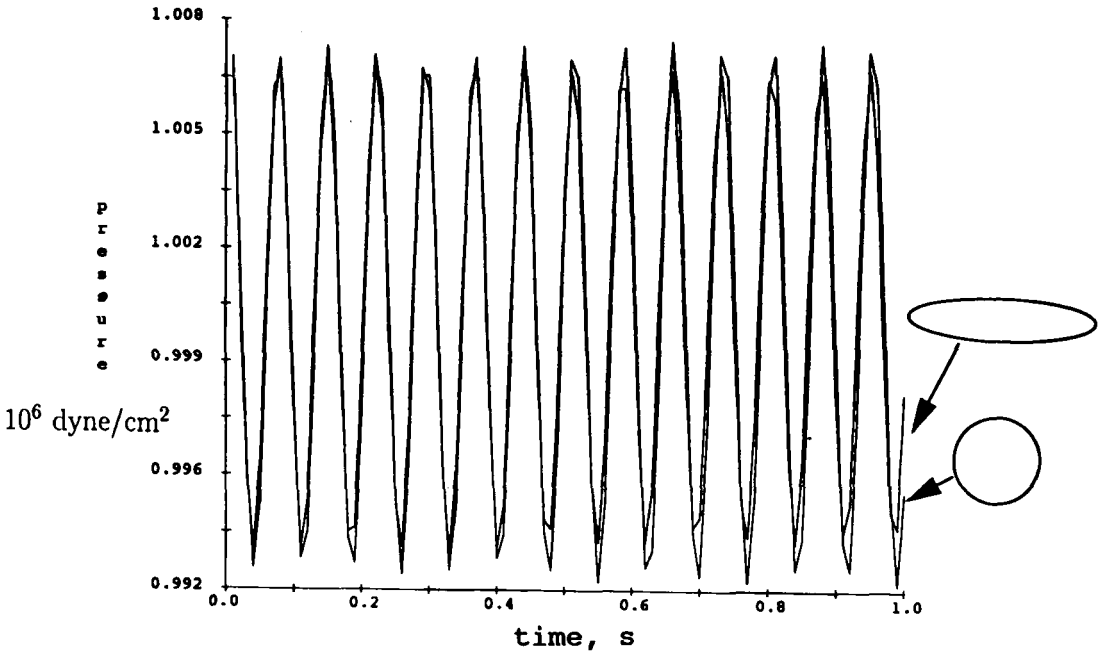

Figure 10. Bubble pressure fluctuations for circular and elliptical (with semi-axis ratio equal to five) bubbles. Explicit formulation, Δt = 0·01 s, zero gravity

where A_0 is the vessel area in the x–y plane and V_0 is the equilibrium bubble volume. The fluid kinetic energy E and the external force work $A^{(e)}$ in the control volume surrounding V_{fl} are

$$\mathrm{d}E/\mathrm{d}t = \rho(A_0 h - \tfrac{1}{2}V_0)\dot{z}\ddot{z}, \tag{25}$$

$$\mathrm{d}A^{(e)}/\mathrm{d}t = p_b \int_\Sigma \mathbf{u}\cdot\mathbf{n}\,\mathrm{d}\sigma - p_0 A_0 \dot{z}, \tag{26}$$

where the integral is taken over the surface of the bubble with the outward normal $\mathbf{n}$. For simplicity the surface tension was not included. Owing to the incompressibility of the fluid, we have

$$\int_\Sigma \mathbf{u}\cdot\mathbf{n}\,\mathrm{d}\sigma = A_0\dot{z}, \tag{27}$$

$$p_b = p_{b_0}(V_0/V)^\gamma = p_{b_0}(V_0/(V_0 + A_0 z))^\gamma. \tag{28}$$

Summarizing equations (25)–(28), for small deviations of the bubble pressure from the equilibrium value $p_{b_0} = p_0$ the equation for z appears similar to equation (7) but with

$$a^2 = p_0\gamma A_0^2/\rho V_0(A_0 h - \tfrac{1}{2}V_0). \tag{29}$$

If the fluid volume is much larger than V_0, then equation (29) for a can be simplified as

$$a^2 = p_0\gamma A_0/\rho V_0 h.$$

In fact, equation (29) for a^2 is a generalization of equation (10) for the planar motion.

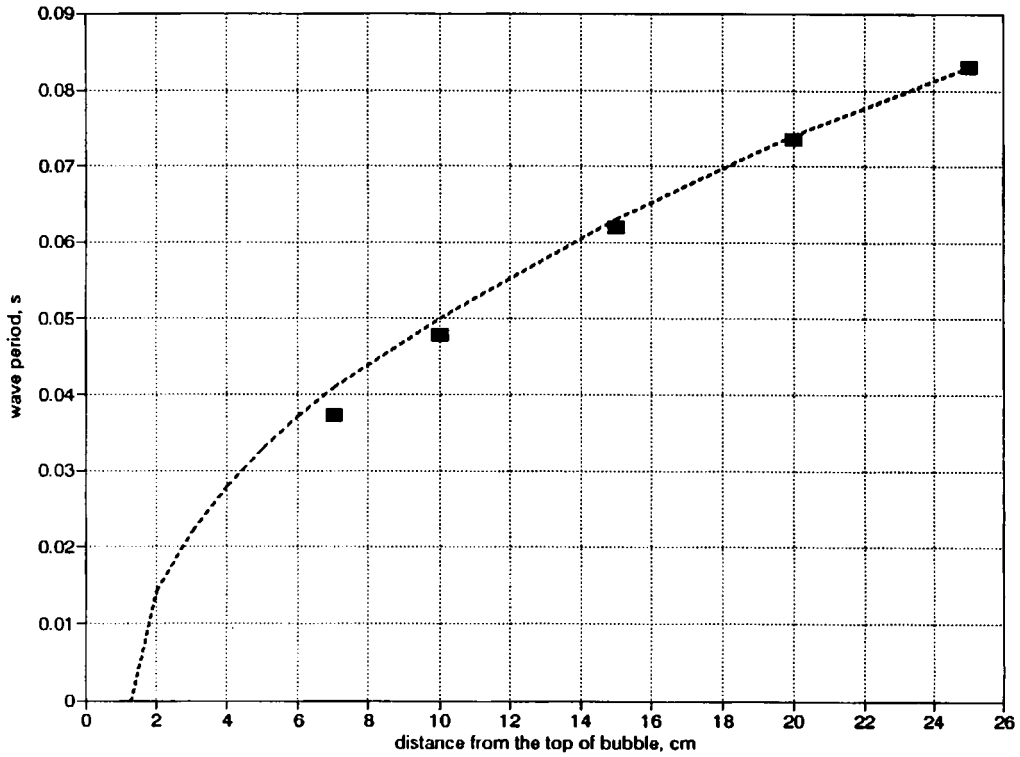

Figure 11. Dependence of 'breathing' wave period $\mathscr{T}$ on distance h for $R_0 = 5$ cm, showing approximate analytical solution (dashed curve) and numerical results (filled squares). Explicit method, $\Delta t = 0{\cdot}01$ s, zero gravity

According to equation (29), the wave period decreases with A_0. However, the larger the area, the less accurate is Assumption 2.

Since the actual shape of the bubble is not specified, this suggests that $\mathscr{T}$ is independent of the bubble shape.

For numerical simulations we will adopt a two-dimensional geometry as before, i.e. infinite dimension in the y-direction. In this case all parameters, including A_0, are calculated per unit length in the y-direction. The dimensions are

$$x_2 - x_1 = 30 \text{ cm}, \qquad z_0 = 32{\cdot}5 \text{ cm}.$$

With the input given by equations (22) and (23) for a circular bubble of radius $R_0 = 5$ cm submerged to a depth $h = 20$ cm we have

$$a = 84{\cdot}57 \text{ s}^{-1}, \qquad \Delta t_{\max} = 0{\cdot}024 \text{ s}, \qquad \mathscr{T} = 0{\cdot}074 \text{ s}.$$

Figure 10 shows that the pressure oscillations for a circular bubble and for an elliptical (semi-axis ratio equal to five) bubble of the same volume (and depth) are similar in both frequency and amplitude. However, the influence of the shape may become important when the bubble size is comparable with the vertical dimension of the fluid and, presumably, if surface tension is present.

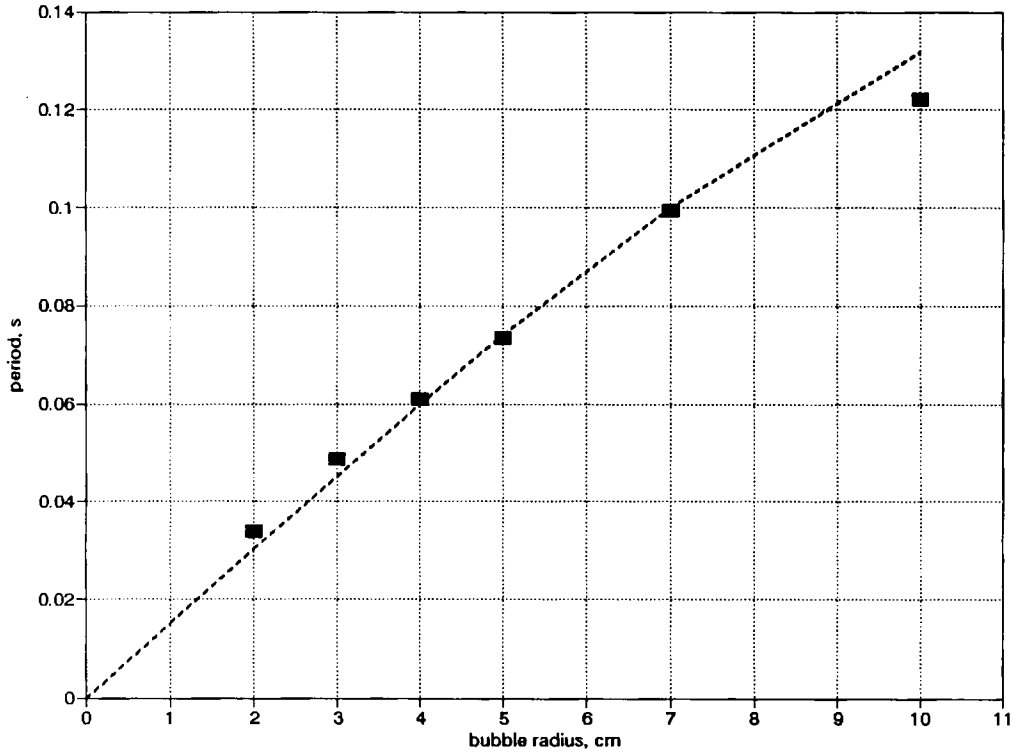

Figure 12. Dependence of 'breathing' wave period $\mathcal{T}$ on equilibrium bubble radius R_0 for $h = 20$ cm, showing approximate analytical solution (dashed curve) and numerical results (filled squares). Explicit formulation, $\Delta t = 0{\cdot}01$ s, zero gravity

Figure 11 shows the variation in $\mathcal{T}$ with h for the circular bubble ($R_0 = 5$ cm) compared with that given by equation (29). The match is better for larger values of the depth because Assumption 2 is more accurate. The minimum value of h is calculated assuming $V_{fl} = 0$, while for the computer simulation h is limited by R_0 and the mesh resolution.

The oscillation period grows with V_0. There will be a larger variation in $\mathcal{T}$ with the radius for spherical bubbles than for a cylindrical one. Figure 12 shows this dependence for a cylindrical bubble at $h = 20$ cm as given by numerical simulations and equation (29). The mismatch for small values of the radius is attributed to the lack of grid resolution. For $R_0 = 2$ cm there are only 4×4 cells to resolve the bubble surface. The approximate analytical solution becomes less accurate for large bubble radii ($R \approx 10$ cm) owing to Assumption 2 and diverges from the numerical result.

If gravity is present, then the waves cannot be considered linear because there is no equilibrium bubble configuration. The overall motion will be a superimposition of non-linear shape deformation waves, volume oscillations and the net upward motion of the bubble, making Assumptions 1 and 2 inappropriate. Besides, the bubble can break up. A sequence of diagrams showing an initially circular 2D bubble floating against the direction of gravity is given in Figure 13. The flow was simulated with $\Delta t = 0{\cdot}01$ s.

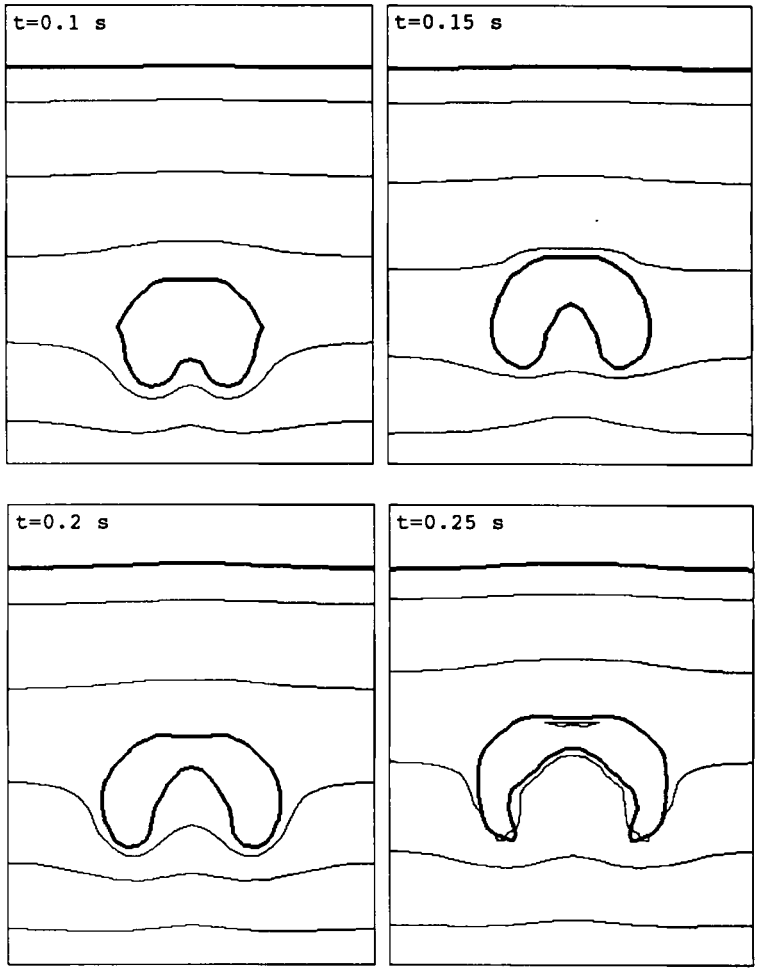

Figure 13. Computer-simulated sequence or a bubble floating upwards in field of gravity. Explicit formulation, $\Delta t = 0{\cdot}01$ s. Thick solid lines mark the free surface and thin lines represent pressure contours

Nevertheless, a few periods of the 'breathing' mode can be observed for the initial 0·25 s as shown in Figure 14(a). Here, as well as in Figures 15 and 16, the pressure is recorded at a point in the fluid and not in the bubble itself. The mean value of the period is about 0·06 s, close to the zero-gravity simulation result.

The time step stability limit varies with the evolution of the bubble, but a sudden and steep decrease in Δt_{max} occurs when the bubble breaks up into three smaller bubbles. This decrease may lead to numerical instability if the time step is not small enough to accommodate this change.

Figure 14(b) shows the evolution of the fluid mean kinetic energy. The onset of instability is clearly seen at the time of break-up. The stability limit here is likely to be dictated by the size of the smallest bubble.

Figure 15 shows the result of the numerical simulation with exactly the same input data as in Figure 14 but using the implicit algorithm. It is clear that the calculation is more stable here,

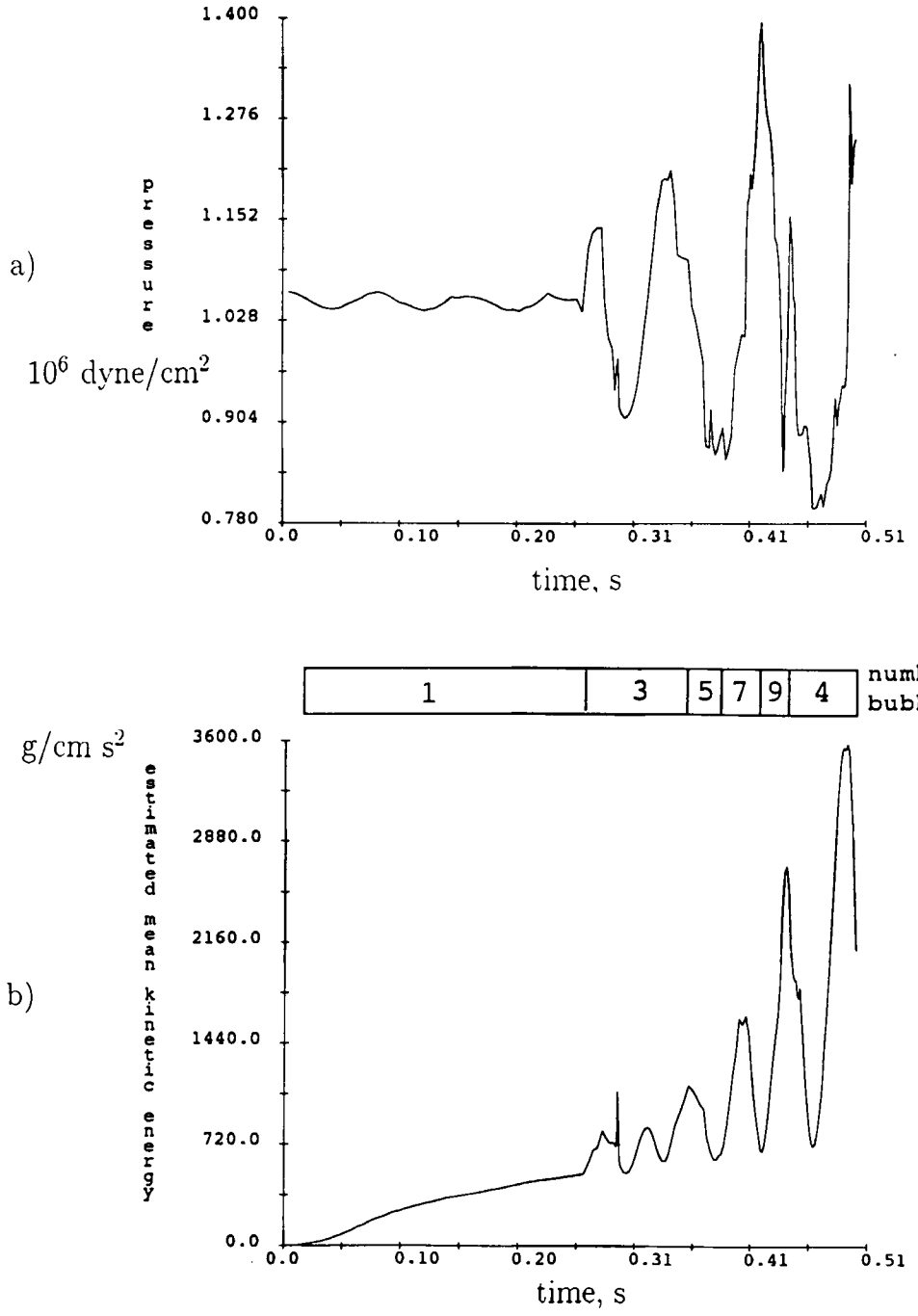

Figure 14. (a) Pressure at a fluid point and (b) mean fluid kinetic energy evolution as the bubble floats upwards, predicted by numerical simulations. Numbers in the bar are the number of bubbles at each time. Explicit formulation, $\Delta t = 0{\cdot}01$ s

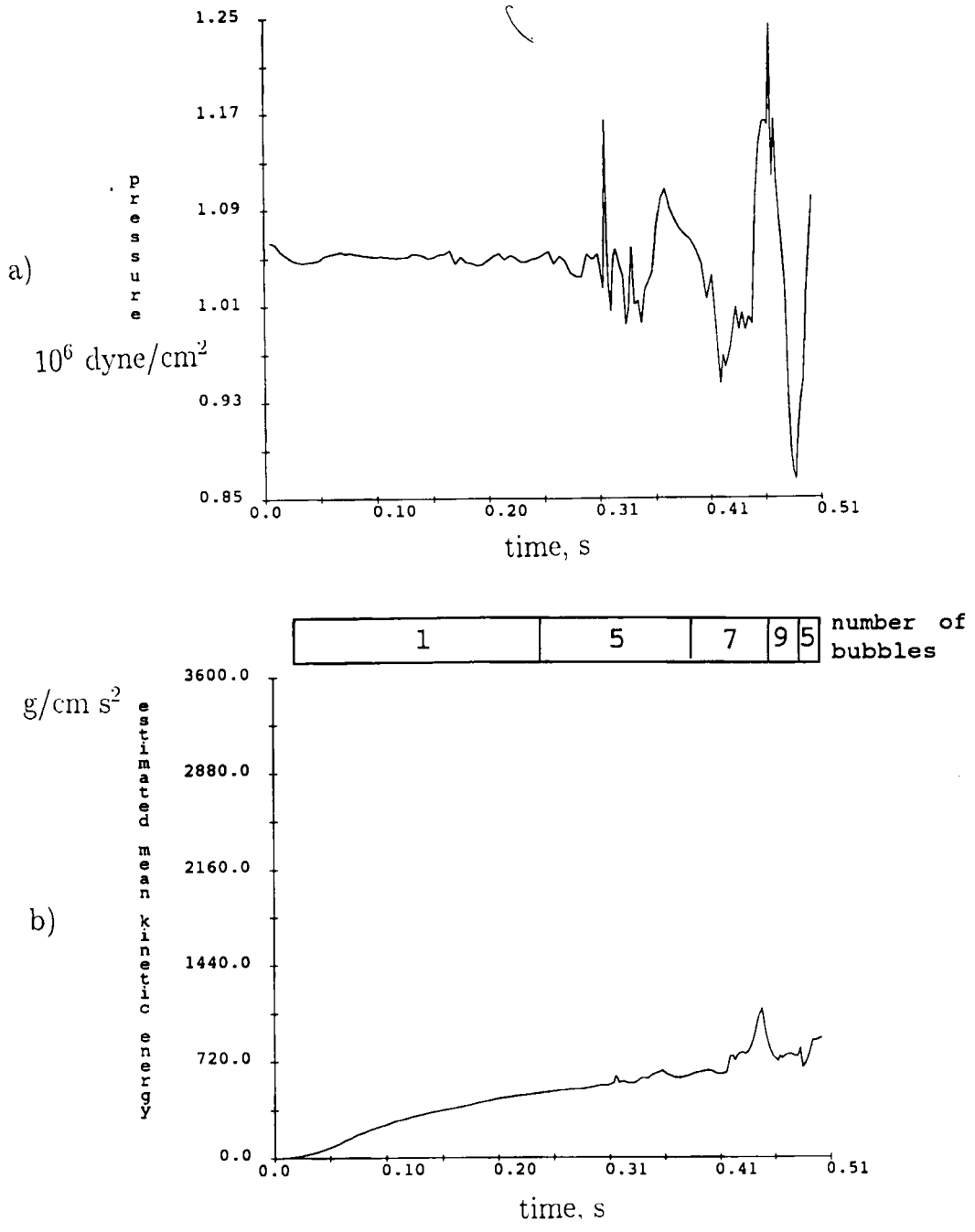

Figure 15. Same as Figure 14 but using implicit method

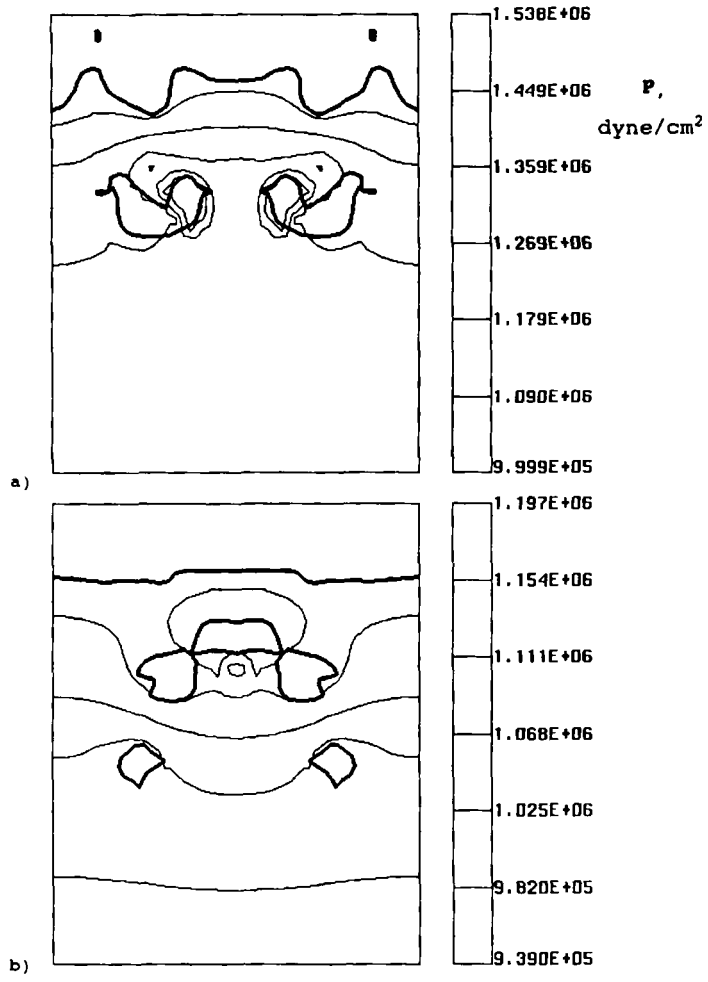

Figure 16. Comparison of pressure distributions and free surface configurations at $t = 0{\cdot}5$ s of simulation for (a) explicit and (b) implicit methods

though some oscillations of the numerical solution can be seen at the end of the calculation. The latter happens because the bubble breaks into up to six smaller ones and the mesh becomes insufficient to resolve them. Truncation errors introduce bubble volume changes which are comparable with the volume itself.

Figure 16 compares the state of the flow at the end of the explicit and implicit calculations at $t = 0{\cdot}5$ s. The result from the implicit method is more physically reasonable when compared with the explicit method results, since

(a) the calculated pressure varies spatially in a narrower range of values
(b) the pressure gradient is more evenly distributed (see pressure contour lines in Figure 16)
(c) the free surface shape is smoother.

The use of the implicit algorithm also gives a shorter computation time, because the smoother flow allows the use of larger time steps.

5. CONCLUSIONS

It has been shown that a numerical instability can develop when modelling gas bubbles in fluids. The instability is associated with the radial or 'breathing' wave mode in which the volume of the bubble oscillates with time. These oscillations lead to bubble pressure fluctuations governed by equation (6).

If in a numerical model this pressure is used as a boundary condition at the fluid free surface surrounding the bubble, then two options are available: explicit or implicit formulation of the boundary condition. Explicit formulation means that during the calculation at a given time step the free surface is kept at its position defined at the previous time step, while in the implicit method the solutions or the free surface position, fluid pressure and velocity are found simultaneously.

The explicit option is conditionally stable, i.e. the time step size is limited to maintain numerical stability. The maximum value of the time step is mesh-independent and is a function of the natural 'breathing' oscillation period. The latter depends on the surrounding fluid inertia m, bubble stiffness γp_{b_0}, bubble volume V_0, and surface tension σ as shown by equation (16).

A method is suggested for finding the stability limit in a situation where no analytical solution is available. It simulates numerically the 'breathing' oscillation mode and finds its period. The maximum time step then can be found from equation (14). However, this approach may not be efficient in situations where the oscillation period changes rapidly or when other oscillation modes interact with the 'breathing' mode.

The implicit method offers unconditional stability but introduces numerical diffusion which depends on the size of the time step.

The numerical results were obtained using the finite volume CFD code FLOW-3D based on the SOLA-VOF method. These results were compared with the exact analytical solution for one-dimensional oscillations and with an approximate analytical solution for a three-dimensional problem. In the latter case the oscillation period (hence the stability limit) does not depend on the bubble shape for a given volume. Both numerical and theoretical results are in close agreement and it is suggested that the simulated instability can be an intrinsic problem for any CFD code which models those oscillations.

Although the stability criterion depends on a variety of physical parameters, it appears to be most sensitive to the bubble volume. This means that bubble break-up is the most significant factor that can lead to instability of a numerical algorithm if the time step is not sufficiently small. This makes it difficult, if at all possible, to find the stability limit in a general case of bubble motion.

It is a result of the present work that the implicit algorithm for bubble modelling has been developed and adopted for FLOW-3D.

ACKNOWLEDGEMENT

This work has been carried out under the research grant GR/34636 awarded by the Application of Computer Modelling in Engineering Directorate of the U.K. Science and Engineering Research Council.

The authors would like to thank Flow Science Inc. for invaluable help and co-operation during the work.

REFERENCES

1. J. K. Walters and J. F. Davidson, 'The initial motion of a gas bubble formed in an inviscid liquid, Pt. 1: The two-dimensional bubble', *J. Fluid Mech.*, **12**, 408–417 (1962).
2. J. K. Walters and J. F. Davidson, 'The initial motion of a gas bubble formed in an inviscid liquid, Pt. 2: The three-dimensional bubble', *J. Fluid Mech.*, **17**, 321–339 (1963).
3. K. Vokurka, 'Amplitudes of free bubble oscillations in liquids', *J. Sound Vibr.*, **141**, 259–275 (1990).
4. J. M. Boulton-Stone, 'A two-dimensional bubble near a free surface', *J. Eng. Math.*, **27**, 73–87 (1993).
5. R. Mei and J. Klausner, 'Unsteady force on a spherical bubble at finite Reynolds number with small fluctuations in the free-stream velocity', *Phys. Fluids A*, **4**, 63–70 (1992).
6. S. M. Yang, Z. C. Feng and L. G. Leal, 'Nonlinear effects in the dynamics of shape and volume oscillations for a gas bubble in an external flow', *J. Fluid Mech.*, **247**, 417–454 (1993).
7. G. Ryskin and L. G. Leal, 'Numerical solution of free boundary problem in fluid mechanisms. Part 1. The finite difference technique', *J. Fluid Mech.*, **148**, 1–17 (1984).
8. G. Ryskin and L. G. Leal, 'Numerical solution of free boundary problem in fluid mechanisms. Part 2. Buoyancy driven motion of gas bubble through a quiescent liquid', *J. Fluid Mech.*, **148**, 19–35 (1984).
9. I. S. Kang and L. G. Leal, 'Numerical solution of axisymmetric, unsteady free-boundary problems at finite Reynolds number. II. Deformation of a bubble in a biaxial straining flow', *Phys. Fluids A*, **1**, 644–660 (1989).
10. K. S. Chan, K. Pericleous and M. Cross, 'Numerical simulation of flows encountered during mould-filling', *Appl. Math. Modell.*, **15**, 624–631 (1991).
11. J. D. Bugg and R. D. Rowe, 'Modelling the initial motion of large cylindrical and spherical bubbles', *Int. j. numer. methods fluids*, **13**, 109–129 (1991).
12. C. W. Hirt and B. D. Nichols, 'Volume of fluid (VOF) method for the dynamics of free boundaries', *J. Comput. Phys.*, **39**, 201 (1981).
13. F. H. Harlow and J. E. Welch, 'The MAC method: a computing technique for solving viscous, incompressible, transient fluid flow problems involving free surfaces', *Phys. Fluids A*, **8**, 2182 (1965).
14. J. Szekely, *Fluid Flow Phenomena in Metals Processing*, Academic, London, 1979.
15. L. I. Sedov, *Mekhanika Sploshnoi Sredy (Continuum Mechanics)*, Nauka, Moscow, 1976.
16. C. W. Hirt, 'Identification and treatment of stiff bubble problems', *Flow Science Inc. communication to FLOW-3D users*, October 1992.
17. J. M. Ortega and W. C. Rheinboldt, *Iterative Solution for Nonlinear Equations in Several Variables*, Academic, New York, 1970.